Genetic and epigenetic changes in clonal descendants of irradiated human fibroblasts

Julia Flunkert[a], Anna Maierhofer[a], Marcus Dittrich[a,b], Tobias Müller[b], Steve Horvath[c], Indrajit Nanda[a], Thomas Haaf[a,*]

[a] *Institute of Human Genetics, Julius Maximilians University, 97074 Würzburg, Germany*
[b] *Department of Bioinformatics, Julius Maximilians University, 97074 Würzburg, Germany*
[c] *Department of Human Genetics, David Geffen School of Medicine, University of California Los Angeles, Los Angeles, CA 90095, USA*

A B S T R A C T

To study delayed genetic and epigenetic radiation effects, which may trigger radiation-induced carcinogenesis, we have established single-cell clones from irradiated and non-irradiated primary human fibroblasts. Stable clones were endowed with the same karyotype in all analyzed metaphases after 20 population doublings (PDs), whereas unstable clones displayed mosaics of normal and abnormal karyotypes. To account for variation in radiation sensitivity, all experiments were performed with two different fibroblast strains. After a single X-ray dose of 2 Gy more than half of the irradiated clones exhibited radiation-induced genome instability (RIGI). Irradiated clones displayed an increased rate of loss of chromosome Y (LOY) and copy number variations (CNVs), compared to controls. CNV breakpoints clustered in specific chromosome regions, in particular 3p14.2 and 7q11.21, coinciding with common fragile sites. CNVs affecting the *FHIT* gene in FRA3B were observed in independent unstable clones and may drive RIGI. Bisulfite pyrosequencing of control clones and the respective primary culture revealed global hypomethylation of ALU, LINE-1, and alpha-satellite repeats as well as rDNA hypermethylation during in vitro ageing. Irradiated clones showed further reduced ALU and alpha-satellite methylation and increased rDNA methylation, compared to controls. Methylation arrays identified several hundred differentially methylated genes and several enriched pathways associated with in vitro ageing. Methylation changes in 259 genes and the MAP kinase signaling pathway were associated with delayed radiation effects (after 20 PDs). Collectively, our results suggest that both genetic (LOY and CNVs) and epigenetic changes occur in the progeny of exposed cells that were not damaged directly by irradiation, likely contributing to radiation-induced carcinogenesis. We did not observe epigenetic differences between stable and unstable irradiated clones. The fact that the DNA methylation (DNAm) age of clones derived from the same primary culture varied greatly suggests that DNAm age of a single cell (represented by a clone) can be quite different from the DNAm age of a tissue. We propose that DNAm age reflects the emergent property of a large number of individual cells whose respective DNAm ages can be highly variable.

1. Introduction

Ionizing radiation plays an important role in medical diagnostics and cancer treatment. Although radiation therapy is targeted to the tumor, it also affects surrounding healthy tissue. Secondary malignancies can manifest as late complications of radiotherapy [1]. Both direct DNA damage (i.e. base damage, single- and double-strand breaks, and DNA-protein crosslinks) in the exposed cells themselves and genome instability in the descendants of cells without direct DNA damage may contribute to radiation-induced carcinogenesis. Numerous in vitro and in vivo studies have shown that radiation-induced genome instability (RIGI), defined by different endpoints (gene mutations and amplifications, cytogenetic abnormalities, micronuclei, and/or delayed cell death) occurs in cells several generations after exposure to low and high-linear energy transfer [2–4]. Although different mechanisms including oxidative stress by mitochondrial dysfunction, cytokine secretion and inflammatory type reactions have been proposed [5–7], the factors for translating the effects of radiation to the non-exposed descendants of irradiated cells remain to be elucidated.

Epigenetic modifications are primary candidates for a radiation memory, which can be transmitted throughout many cell divisions to the clonal progeny of an exposed cell. Previously we have shown that

---

global DNA methylation remains rather stable in normal body cells (primary fibroblasts) within the first cell cycle after irradiation [8]. Accumulating evidence suggests that irradiation is associated with global and gene-specific DNA methylation alterations several population doublings (PDs) after radiation exposure [9–14]. This is consistent with the idea that irradiation interferes with the epigenetic maintenance system. Similar to RIGI, radiation-induced epigenetic instability may play a major role in carcinogenesis among survivors of cancer therapies.

Epigenetic processes are crucial for maintaining cellular homeostasis. Promoter methylation during development, differentiation, and disease processes leads to an inactive chromatin structure, whereas gene body methylation is associated with active genes [15]. In addition, methylated CpGs are enriched in repetitive DNA elements to prevent retrotransposition activity [16]. DNA methylation is dramatically altered in cancer cells, interfering with genome stability. Both silencing of tumor suppressor genes by promoter hypermethylation and reactivation of retrotransposons by repeat hypomethylation cause genome instability [17,18]. Compared to methylation, hydroxymethylation is a relatively rare DNA modification that is found in different mammalian tissues with the highest concentration in brain [19]. Oxidation of 5-methylcytosine (5-mC) to 5-hydroxymethylcytosine (5-hmC) is catalyzed by the TET family of enzymes and may be involved in epigenetic gene regulation [20].

To study epigenetic instability in normal body cells with intact DNA repair and cell cycle checkpoints, we have established single-cell clones from irradiated and non-irradiated human embryonal fibroblast strains. Chromosome banding analysis was performed after 20 PDs to identify stable and unstable clones. Epigenetic changes between control clones and the respective primary fibroblast culture are the result of in vitro ageing. Comparison of irradiated vs. control clones and stable vs. unstable clones reveals radiation-induced epigenetic effects which may contribute to RIGI and carcinogenesis. In addition to global and gene-specific methylation patterns, we have screened clones for de novo copy number variations (CNVs). CNVs have been associated with various human diseases including cancer [21,22]. In contrast, little is known about the role of radiation-induced CNVs in carcinogenesis. Irradiation of transformed fibroblasts induced CNVs in a dose-dependent manner with hotspots in regions sensitive to replication stress [23].

2. Material and methods

2.1. Cell culture

Human primary fibroblast strains were established from excess materials of amniocenteses from two human male fetuses without phenotypic and chromosomal abnormalities. Cells were cultured in T25 flasks in Chang Medium with L-glutamine (Irvine Scientific, CA, USA) at 37 °C in an incubator with 5% CO_2 atmosphere. Medium was changed one day before irradiation. Subconfluent cultures were exposed at room temperature to a single X-ray dose of 2 Gy (8 Gy/min) using a Siemens Primus L linear accelerator (Siemens, Concord, CA, USA). Twenty-four hours after irradiation 300 cells each were plated in 100 mm petri dishes. Non-irradiated cells were plated as controls. Cells were grown until colonies became visible. Individual colonies were isolated using cloning rings and serially expanded, first in well plates and then in culture flasks. After expansion for 20 PDs, cells from single-cell clones were harvested for DNA isolation and chromosome preparation.

2.2. Classical and molecular cytogenetic analyses

Chromosomes were prepared from exponentially growing fibroblast cultures and analyzed by G-banding [24], using conventional techniques. Metaphases were systematically scored for chromatid and chromosome breaks, terminal and interstitial deletions, inversions, translocations, isochromosomes, derivative chromosomes, additional

material of unknown origin, and aneuploidies. Clones with a normal karyotype in all (at least 10) analyzed metaphases were considered as stable and clones presenting a mixture of cells with different (usually normal and abnormal) karyotypes as unstable. If the same aberration, i.e. a translocation was found in all cells of a given clone, it resulted from direct DNA damage in the irradiated cell. Then the clone was classified as stable or unstable depending on the remaining chromosomes. To avoid misclassifications due to metaphase spreading artefacts, monosomies were only considered as radiation-induced aneuploidy if the same chromosome was lost in at least three metaphases of a given clone.

Interphase fluorescence in situ hybridization (FISH) was performed with the CEP X SpectrumOrange/Y SpectrumGreen DNA Probe Kit (Abbott Laboratories, Illinois, USA), using standard FISH protocols [25]. Chromosome-specific alpha satellite DNA (DXZ1) at the X centromere and satellite III DNA (DYZ3) at the Y long arm allowed rapid enumeration of sex chromosomes in interphase nuclei.

Genomic DNA was isolated with the Quick-gDNA MiniPrep Kit (Zymo Research, Irvine, CA, USA). DNA concentration was quantified using a Qubit Fluorometer (ThermoFisher Scientific, Waltham, USA). HumanCytoSNP-12 DNA BeadChips (Illumina, San Diego, CA, USA) were used to assess CNVs in irradiated and non-irradiated fibroblast clones. Assays were performed according to manufacturer's instructions with 250 ng genomic DNA each. BeadChips were scanned with an Illumina iScan. cnvPartition/GenomeStudio Software (Illumina) and BlueFuse Multi Software (Illumina) were used for CNV calling. Chromosome ideograms were generated with the PhenoGram visualization tool (http://visualization.ritchielab.psu.edu/phenograms/plot).

Multiplex ligation-dependent probe amplification (MLPA) [26] with the SALSA MLPA probemix P063-B1 FHIT-WWOX (MRC-Holland, Amsterdam, The Netherlands) and 60 ng input DNA were used to determine copy number changes affecting the *FHIT* gene. The resulting PCR products were separated by capillary electrophoresis on an ABI 3130XL Genetic Analyzer (Applied Biosystems, Darmstadt, Germany). Data were analyzed using Coffalyser.Net software (MRC-Holland, Amsterdam, Netherlands).

2.3. Bisulfite pyrosequencing

Bisulfite conversion of genomic DNA (500 ng aliquots) was performed with the EZ DNA Methylation kit (Zymo Research) according to the manufacturer's protocol. For ALU, LINE-1, and alpha-satellite DNA, first a multiplex PCR amplifying all three repetitive elements was carried out, followed by separate second-round nested PCRs for ALU, LINE-1, and alpha-satellite DNA [8]. In addition, two amplicons were generated from the rDNA promoter, region 1 covering the distal rDNA promoter and region 2 the core promoter element and the upstream control element [27,28]. The PyroMark Assay Design 2.0 software (Qiagen, Hilden, Germany) was used to design PCR and sequencing primers (Supplementary Table S1a). Amplifications were performed with an initial denaturation step at 95 °C for 5 min, followed by a repeat-specific number of cycles of 95 °C for 30 s, specific annealing temperature for 30 s, 72 °C for 45 s and a final extension step at 72 °C for 5 min (Supplementary Table S1b–d). Bisulfite pyrosequencing was done on a PyroMark Q96MD pyrosequencing system (Qiagen) using the PyroMark Gold Q96 CDT reagent kit (Qiagen). The Pyro Q-CpG software (Qiagen) was used for data analysis.

2.4. Methylation array analysis

Samples were run on Infinium HumanMethylation450K BeadChips (Illumina) and scanned with an iScan following the manufacturer's instructions. More than 485,000 CpG sites were targeted, covering 96% of CpG islands (CGIs) and 99% of RefSeq genes with promoter, first exon, gene body, 5' and 3' untranslated regions (UTRs). Array data (NCBI Gene Expression Omnibus no. GSE112877) were analyzed with the

Chip Analysis Methylation Pipeline (ChAMP) [29]. Data were loaded from idat files with the champ.load() function which is utilizing minfi and some filtering steps [30]. Probes with a detection $p > 0.01$, less than three beads in at least 5% of samples, non-CpG cytosines, known SNPs [31], multi-hits, and localization on X and Y were removed. After quality control checks the default type-2 probe correction method beta-mixture quantile (BMIQ) was used for normalization [32]. Batch effects were detected with the singular value decomposition method and corrected with Combat as implemented in the Surrogate Variable Analysis package [33]. Differentially methylated positions (DMPs) were identified with the champ.DMP() function, implementing the limma package. *P* values for differential methylation were calculated using a linear model [34,35]. All *p* values have been corrected for multiple testing using the Benjamini-Hochberg method [36].

2.5. Epigenetic skin and blood clock

The original epigenetic clock is defined as a weighted average across 353 CpG sites and is a multi-tissue predictor of age allowing the estimation of the DNA methylation (DNAm) age of most tissues and cell types. However, in dermal fibroblasts DNA methylation age is poorly calibrated [37]. A newly developed DNA age estimator for skin and blood cells was used that is based on 391 CpGs and applies to various cells including fibroblasts, keratinocytes, buccal cells, and blood cells [38]. The resulting age estimate is referred to as "DNAm age" or "epigenetic age". The output age estimates are in units of years and were multiplied by 365 to get them in units of days.

2.6. Statistical analyses

Statistical analyses were performed using SPSS statistics 24 (IBM, Armonk, NY, USA). *P* values below 0.05 were considered as significant. Fisher´s exact test was used to compare the rate of stable vs. unstable clones and the frequency of clones with LOY between irradiated and non-irradiated cells. It was also used to test for enrichment of radiation-induced CNVs in regions that have been linked to fragile sites [39]. The nonparametric Mann-Whitney *U* test was used to compare the frequency of aberrant metaphases and CNVs per clone between groups. The Kolmogorov-Smirnov test was used to compare CNV size distribution between stable and unstable clones. Spearman rank correlation was used to measure the strength of association between two variables. For pyrosequencing and DNAm age data, the one-sample Wilcoxon signed rank-test was used to compare control clones and mass culture and the Mann-Whitney *U* test to compare control and irradiated clones. Levene's test was used to compare the variances of DNAm age between control and irradiated clones. Gene set enrichment analysis was done using the Enrichr tool (http://amp.pharm.mssm.edu/Enrichr/) [40,41].

3. Results

3.1. Classical chromosome analyses

Following irradiation with 2 Gy, cells from two male human fibroblast strains were clonally expanded for 20 PDs and at least 10 (on average 13) metaphases per clone were analyzed by classical G-banding. Clones derived from non-irradiated cells of the same two strains were used as controls for the effects of in vitro ageing. Altogether we obtained 37 clones from irradiated cells and 12 control clones from strain 1. The majority (27 of 37; 73%) of irradiated clones was unstable, whereas most (9 of 12; 75%) control clones were stable. As expected, unstable clones were significantly (Fisher's exact test; $p = 0.005$) more frequent after irradiation. Similarly, 10 of 19 (53%) clones from irradiated cells but only 3 of 10 (30%) control clones derived from strain 2 were unstable. On average, strain 1 displayed 1.6 aberrant metaphases per clone in irradiated clones, compared to 0.3 in control clones (Mann-Whitney *U* test; $p = 0.003$). Strain 2 was endowed
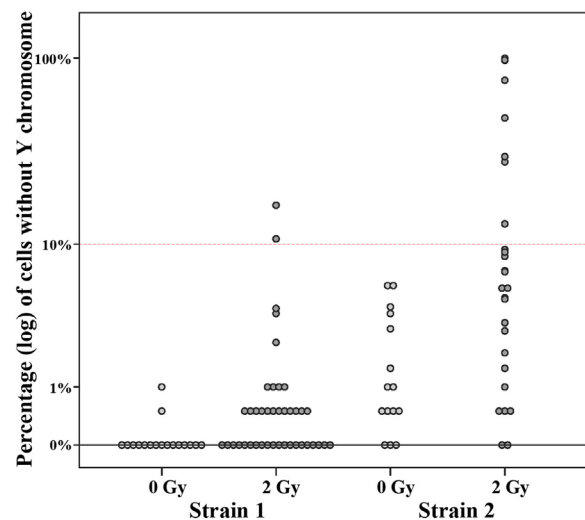

Fig. 1. Percentage of cells without Y chromosome in control clones (0 Gy) and irradiated (2 Gy) clones. Each circle represents an individual clone.

with 1.3 aberrant metaphases per clone in irradiated clones and 0.4 in controls. In both strains and in both stable and unstable clones, the most frequently (40–60%) observed aberrations were chromatid and chromosome breaks. In strain 1 the number of observed aberrations correlated with chromosome size. In strain 2 50% of aberrations affected chromosomes 1, 5, 7, and 12.

3.2. Loss of chromosome Y (LOY)

It is noteworthy that 3 of 19 irradiated clones (but none of the control clones) of strain 2 showed LOY in all analyzed metaphases. LOY was not observed in strain 1. None of the 78 clones from both strains analyzed by G-banding showed comparable loss of the X chromosome or an autosome. To provide additional evidence for radiation-induced LOY, 68 independent clones from irradiated cells and 32 control clones, which had not been used for G-banding, were analyzed by interphase FISH with X and Y enumeration probes. Clones with more than 10% (of at least 200 analyzed) nuclei without a Y signal were considered as LOY-positive. Using this classification, 2 of 41 (5%) irradiated clones from strain 1 and 6 of 25 (24%) from strain 2 but none of the control clones showed LOY (Fig. 1). Consistent with the results of G-banding, strain 2 appeared to be more prone to LOY, exhibiting a significant difference (Fisher's exact test, $p = 0.017$) between irradiated and control clones. None of the analyzed clones showed mosaic loss of the X chromosome.

3.3. Copy number variation

To detect submicroscopic deletions and duplications, 36 irradiated clones (10 stable and 26 unstable) and 10 control clones (7 stable and 3 unstable) from strain 1 as well as 36 irradiated clones (9 stable, 10 unstable, and 17 unclassified) and 12 control clones (7 stable, 3 unstable, and 2 unclassified) from strain 2 were analyzed with HumanCytoSNP-12 DNA BeadChips. All clones derived from strain 1 were endowed with microduplications in chromosome 9q34.11 and 11p15.4, clones from strain 2 with CNVs in 2p11.2, 3p13, 11p11.21, 14q32.33, and 16p13.2. These strain-specific CNVs were already present in the primary cultures. Only de novo CNVs, which arose after irradiation during single-cell cloning and are, therefore, specific for an individual clone(s) were considered for further analysis (Supplementary Table S2). On average 0.2 de novo CNVs per clone were detected in control clones of strain 1 and 0.08 in strain 2. The de novo CNV rate was approximately threefold increased in irradiated clones of strain 1
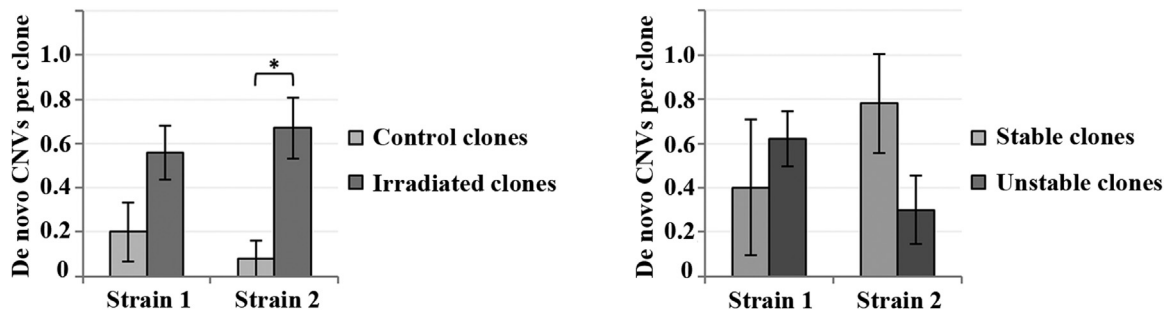
Fig. 2. Frequency of de novo CNVs per clone in irradiated vs. control clones (left diagram) and stable vs. unstable clones (right). Bar diagrams present mean and standard error. Asterisk indicates a significant between-group difference.

and eightfold in strain 2. In strain 2 there was a significant (Mann-Whitney U test, $p = 0.009$) difference between irradiated and control clones (Fig. 2). The comparison between stable and unstable clones did not yield consistent results. In strain 1 unstable clones displayed a slightly increased (0.62 vs. 0.40) de novo CNV rate, whereas in strain 2 stable clones exhibited more de novo CNVs (0.78 vs. 0.30). Of 44 observed radiation-induced CNVs in both strains 23 were deletions and 21 duplications. In addition to CNVs, we identified three regions with mosaic copy-neutral loss of heterozygosity.

The three de novo CNVs in control clones were 184 kb, 367 kb, and 381 kb in length. CNVs in irradiated clones had a median size of 452 kb and an interquartile range (IQR) of 939 kb. CNV size did not significantly (Kolmogorov-Smirnov test) differ between stable (median 582 kb, IQR 767 kb) and unstable clones (median 407 kb, IQR 968 kb). Enrichment analysis of genes affected by de novo CNVs (Supplementary Table S2) did not reveal significantly enriched pathways.

Fig. 3 shows the chromosomal distribution of the 47 identified de novo CNVs (44 in irradiated and 3 in control clones). There is an obvious clustering of independent CNVs in chromosome 3p14.2 and 7q11.2, coinciding with the cytogenetic localization of the common fragile sites 3B and 7J. Clusters were defined by overlapping or closely adjacent (within 1 Mb) CNVs. In addition, the fragile sites 1I, 4D, 6B, 8D, 10C, and 10F were associated with 1–2 CNVs each. Consistent with a previous study [23], our results suggest that chromosome 7q11.2 is particularly susceptible to radiation-induced chromosome instability. However, only 1 of 6 radiation-induced microdeletions involving 7q11.2 and a closely adjacent microdeletion in 7p12.1-7q11.1

contained genes (Supplementary Table S2). Notably, three radiation-induced CNVs (two microdeletions and one duplication) overlapped with chromosome 3p14.2, two of them including sequences of the fragile histidine triad (*FHIT*) gene in FRA3B. An additional micro-duplication was observed in 3p14.1. Interestingly, all three CNVs affecting 3p14.2 and directly or indirectly the *FHIT* gene were found in unstable clones. Therefore, we analyzed *FHIT* copy number by MLPA in 74 independent irradiated clones and identified one additional clone with a heterozygous loss of *FHIT* exon 4. Unfortunately, there was not enough material available to classify this clone by G-banding or array analysis.

3.4. DNA methylation of repetitive elements

Prolonged culture of primary fibroblasts is commonly used as in vitro model system for cellular ageing [42,43]. To study the effects of in vitro ageing, global methylation of different repetitive elements (ALU, LINE-1, alpha-satellite, and rDNA) was compared between control clones at 20 PDs (12 of strain 1 and 20 of strain 2) and the respective primary cultures (duplicates) (Table 1). For both strains, average methylation levels of ALU, LINE-1, and alpha-satellite DNA were significantly reduced in control clones compared to primary culture. With 4.9% in strain 1% and 6.9% in strain 2, age-related hypomethylation was most pronounced (Wilcoxon signed rank-test; $p = 0.004$ and $p < 0.001$) for alpha-satellite DNA. ALU methylation levels were reduced by 0.8% ($p = 0.012$) and 0.7% ($p = 0.005$), LINE-1 by 2.4% ($p = 0.010$) and 1.9% ($p = 0.002$) in strain 1 and 2, respectively. In

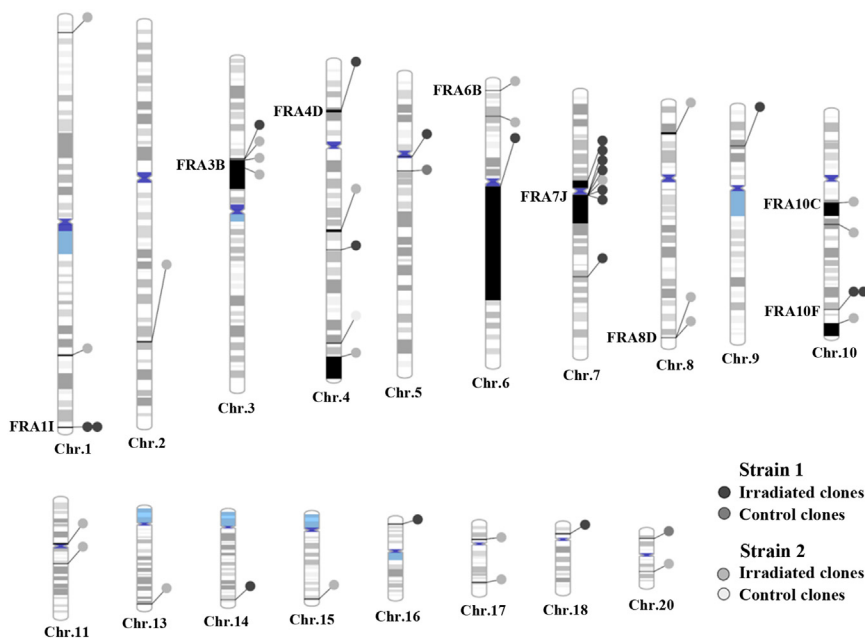**Fig. 3.** Chromosomal location of CNVs. Chromosomes without CNVs are not depicted. Circles in different shades of grey indicate irradiated and control clones from strain 1 and 2, respectively. Black bars in the chromosome ideograms indicate cytogenetically visible large CNVs, the largest on chromosome 6 spanning 85 Mb. The fragile sites indicated on the left side of the ideograms overlap with CNVs.

Table 1

Mean DNA methylation of repetitive DNA elements.

		Alpha-satellite			ALU			LINE-1			rDNA region 1			rDNA region 2		
		n	Mean	SE	n	Mean	SE	n	Mean	SE	n	Mean	SE	n	Mean	SE
Strain 1	Primary culture[a]	1	78.4	0.9	1	25.3	0.1	1	78.9	0.6	1	13.0	0.5	1	16.4	0.6
	Control clones	12	73.5	1.0	12	24.5	0.3	12	76.5	0.7	12	16.6	0.8	12	21.4	0.8
	Irradiated clones	34	68.1	0.6	33	23.6	0.2	34	76.1	0.3	32	17.8	0.3	34	22.7	0.3
	Stable	9	67.7	1.1	9	23.7	0.3	9	75.6	0.5	8	16.9	0.3	9	22.0	0.5
	Unstable	25	68.3	0.7	24	23.6	0.2	25	76.3	0.4	24	18.1	0.3	25	22.9	0.3
Strain 2	Primary culture[a]	1	84.6	0.3	1	26.5	1.0	1	74.5	1.3	1	19.1	0.1	1	24.5	0.4
	Control clones	20	77.7	0.4	20	25.8	0.2	20	72.6	0.6	15	20.9	0.4	20	27.5	0.5
	Irradiated clones	26	77.1	0.6	26	25.6	0.2	26	72.6	0.5	19	21.0	0.3	26	27.9	0.4
	Stable	8	76.5	1.6	8	25.6	0.4	8	73.1	1.1	7	21.0	0.5	8	27.9	0.7
	Unstable	10	77.6	0.6	10	25.6	0.3	10	71.3	1.0	7	20.8	0.6	10	27.6	0.5

[a] Duplicate measurements.

contrast, rDNA promoter methylation increased with in vitro ageing in both strains. 3.6% ($p = 0.005$) and 1.8% ($p = 0.001$) increments were observed in region 1 and 5.0% ($p = 0.003$) and 3.0% ($p < 0.001$) in region 2.

To study radiation effects, irradiated clones (34 of strain 1 and 26 from strain 2) were compared to control clones (12 and 20, respectively) (Table 1). In irradiated clones of strain 1, ALU methylation was decreased by 0.9% (Mann-Whitney U test, $p = 0.015$) and alpha-satellite DNA methylation by 5.4% ($p < 0.001$). rDNA promoter methylation was increased by 1.2% (region 1) and 1.3% (region 2), showing a trend difference ($p = 0.068$ and $p = 0.061$, respectively). In strain 2, changes were in the same direction but not significant. When comparing stable and unstable irradiated clones from strain 1 (9 vs. 25) and strain 2 (9 vs. 10), none of the analyzed repeat families revealed a significant between-group difference.

3.5. Methylation arrays

The same clones and primary cultures that have been analyzed by bisulfite pyrosequencing were used for methylation array analyses. Comparison of control clones and primary culture revealed 6277 significant (FDR-adjusted $p < 0.05$) DMPs (4566 annotated to 3396 different genes) and 19,281 DMPs (13,452 annotated to 7138 genes) for strain 1 and 2, respectively. The 1131 DMPs (Supplementary Table S3) that were differentially methylated in both strains were used for further analysis. The β differences of overlapping DMPs in strain 1 and 2 were positively correlated (Spearman-Rho 0.7, $p < 0.001$). Enrichment analysis of the 667 genes annotated to overlapping DMPs revealed several pathways with a FDR-adjusted $p < 0.08$ (Table 2). "Focal adhesion", "RAS signaling", "PI3K-AKT signaling", "AMPK signaling", "synaptic vesicle cycle", "central carbon metabolism", and "galactose metabolism" all have been associated with ageing and/or ageing-related diseases in the literature [44–52]. Sixteen of the 667 genes with in vitro ageing-related DMPs (A2M, AKT1, ATM, BRCA1, FGFR1, HIC1, HOXC4, HSF1, IGF1R, IRS1, KCNA3, NCOR2, NUDT1, PPARGC1A, RB1, and RECQL4) in our study are also contained in a list of 307 genes in the Ageing Gene Database (http://genomics.senescence.info/genes/), which is a significant (Fisher's exact test; $p = 0.047$) overlap.

The comparison of irradiated vs. control clones is consistent with large epigenetic drift after irradiation. Strain 1 displayed 34,515 radiation-sensitive DMPs (24,152 annotated to 10,872 genes) with an FDR-adjusted $p < 0.001$. Enrichment analysis of 2757 genes with at least 2 DMPs yielded 62 significant (FDR-adjusted $p < 0.05$) pathways. The top 10 including "pathways in cancer" and different (Calcium, Rap1, PI3K-Alt, MAPK, and Ras) signaling pathways are presented in Table 2. Consistent with interindividual differences in the cellular response to radiation-induced damage [53], only 4452 significant DMPs (3324 annotated to 2761 genes) with an FDR-adjusted $p < 0.05$ were identified in strain 2. In both strains > 60% of DMPs were

hypomethylated in irradiated clones. A limited number of 396 DMPs (annotated to 259 genes) was overlapping in both strains (Supplementary Table S4). There was a positive correlation (Spearman-Rho 0.2, $p < 0.001$) between the corresponding β values in strain 1 and 2. Genes associated with the "MAPK signaling pathway" were significantly (FDR-adjusted $p = 0.02$) enriched in these 259 overlapping genes. Comparison of the methylation data sets from unstable vs. stable clones did not reveal any significant DMPs.

3.6. DNA methylation age

DNAm age is known to correlate strongly with chronological age across a broad spectrum of tissues and cell types and applies to the entire age range (from fetal development to centenarians) [37]. According to the new epigenetic clock for skin and blood cells [38], fetal fibroblasts from primary cultures displayed a negative mean DNAm age of − 228 ± 24 days in the first and − 209 ± 1 days in the second strain. After 20 PDs control clones exhibited increased mean DNAm ages of − 206 ± 37 days and − 160 ± 112 days, respectively, showing a trend towards significance (Wilcoxon signed rank test; $p = 0.084$ and $p = 0.057$). Irradiated clones had a mean DNAm age of − 198 ± 86 days and − 138 ± 123 days, being on average 8 days and 22 days older than the respective control clones (Fig. 4). Notably, there was an enormous variation of DNAm age between clones (all at 20 PDs) in both the control (range − 271 to − 160 days in strain 1 and − 251 to 258 days in strain 2) and the irradiated group (− 324 to − 31 days in strain 1 and − 306 to 200 days in strain 2). For strain 1, the variances of control clones and irradiated clones were significantly (Levene's test; $p = 0.003$) different. This is consistent with the view that irradiation increases DNAm age variation between clones. In fact some clones at 20 PDs were epigenetically younger than the respective primary culture. Compared to stable clones, unstable clones were on average 40 days younger in strain 1 and 67 days younger in strain 2 (Mann-Whitney U test; $p = 0.216$ and $p = 0.068$). In stable clones the DNAm age ranged from − 324 to − 53 days in strain 1 and from − 281 to 30 days in strain 2. Unstable clones displayed DNAm ages from − 312 to − 31 days in strain 1 and from − 306 to 30 days in strain 2.

4. Discussion

4.1. Limitations

Tumorigenesis is a multistep process, involving an accumulation of genetic and epigenetic alterations in multiple genes [54,55]. To study radiation-induced changes during clonal evolution of irradiated normal body cells, we have used an in vitro model based on single-cell clones from irradiated primary fibroblasts. Single-cell clones from non-irradiated cells of the same strains served as controls for ageing-related alterations. Following irradiation with 2 Gy the number of unstable

Table 2
Enrichment analysis using genes with DMPs associated with in vitro ageing and irradiation.

Contrast	Term		Overlap	Adjusted p value	Comb. score	Overlapping genes
In vitro ageing	Focal adhesion	hsa04510	17/202	0.079	14.8	TNXB, ACTN2, LAMC3, SRC, THBS2, VAV2, IGF1R, COMP, CCND3, COL4A2, COL4A1, PDGFD, COL6A2, RAC2, AKT1, DOCK1, BCAR1
	Ras signaling	hsa04014	17/227	0.079	12.5	BRAP, ANGPT4, RAB5C, RASGRF2, CALML3, GRIN1, IGF1R, PLD2, RASA3, GNG7, PDGFD, KIT, RAC2, AKT1, GNB3, FGFR2, FGFR1
	PI3K-Akt signaling	hsa04151	22/341	0.079	11.4	ANGPT4, TNXB, IRS1, LAMC3, BRCA1, THBS2, IGF1R, RPTOR, COMP, CCND3, COL4A2, COL4A1, CREB3L1, GNG7, PDGFD, COL6A2, KIT, AKT1, GNB3, FGFR2, FGFR1, CREB5
	Synaptic vesicle cycle	hsa04721	8/63	0.079	11.3	RAB3A, AP2A1, SLC17A7, SLC17A8, CPLX1, AP2A2, SLC18A2, AP2M1
	Central carbon metabolism in cancer	hsa05230	8/67	0.079	11.2	PFKL, HKDC1, KIT, AKT1, FGFR2, PFKP, HK1, FGFR1
	AMPK signaling	hsa04152	11/124	0.079	9.3	RPTOR, PFKL, IRS1, CREB3L1, AKT1, CPT1C, PPARGC1A, ADRA1A, PFKP, CREB5, IGF1R
	Galactose metabolism	hsa00052	5/30	0.079	7.4	PFKL, HKDC1, LALBA, PFKP, HK1
Irradiation (strain 1)	Pathways in cancer	hsa05200	101/397	7.4E−08	46.0	RB1, SPI1, CSF3R, HHIP, ITGA2B, FGF1, FGF2, ETS1, IGF1R, RASSF1, EDNRB, CCND1, AKT2, PRKACA, PDGFRB, WNT5B, PRKCB, DAPK1, WNT5A, PRKCA, MITF, BCR, ADCY9, COL4A2, COL4A1, AGTR1, CSF1R, CTBP2, CTBP1, EPAS1, PDGFB, PLD1, WNT6, FGF20, FADD, WNT4, STAT5A, CREBBP, WNT10A, SMAD5, WNT3A, ZBTB16, FZD6, BRAF, IGF1, GNG12, NFKB1, CDK6, FGF14, GNB1, BCL2, GNAS, GRB2, FGF12, FGFR3, FGFR2, CDKN1A, HSP90AB1, PIK3CD, GLI3, GLI2, MECOM, BDKRB2, BDKRB1, JAK1, APC2, PLEKHG5, NCOA4, TGFBR2, CCNA1, PAX8, TRAF3, RARA, ITGA6, BIRC7, MET, PPARD, LAMA2, HDAC1, PTGER3, LAMA3, ADCY4, ADCY2, ADCY8, ADCY6, EGFR, RXRB, RXRA, GNG7, GNA12, CTNNA3, CTNNA2, RUNX1T1, NTRK1, TCF7L1, TCF7L1, LAMB3, PML, VEGFA, MAPK10, KRAS
	Calcium signaling	hsa04020	57/180	7.4E−08	41.3	CHRM2, RYR1, RYR2, OXTR, HTR2A, RYR3, SLC8A2, EDNRB, BDKRB2, PLCE1, BDKRB1, NOS1, PRKACA, PDGFRB, PRKCB, SPHK2, PRKCA, TACR1, ITPKB, ADCY9, STIM1, LTB4R2, CCKBR, ORAI2, AGTR1, CAMK2B, PDE1A, PTGER3, ADCY4, CACNA1B, ITPR1, CACNA1A, ADCY2, CACNA1D, CACNA1C, ADCY8, CACNA1E, EGFR, CACNA1H, CACNA1G, CACNA1I, GRIN2A, GNA15, PHKG1, PTK2B, NOS3, ATP2B2, GRIN2C, HTR5A, GRIN2D, GRIN1, P2RX5, P2RX3, P2RX1, GNAS, PLCD1
	Rap1 signaling	hsa04015	62/211	1.9E−07	37.3	DOCK4, FLT4, ITGA2B, ITGB2, PIK3CD, SIPA1L2, FGF1, ITGAL, FGF2, IGF1R, AKT2, PLCE1, PDGFRB, MAGI1, PRKCB, MAGI2, PRKCA, VAV2, APBB1IP, ADCY9, PARD3, PRKD2, RAPGEF5, MET, SKAP1, RAPGEF4, CSF1R, SRC, ADCY4, PDGFB, ADCY2, ADCY8, PRKCZ, ADCY6, EGFR, RAP1GAP, GRIN2A, CNR1, PDGFD, PDGFC, FGF20, MAP2K6, FARP2, NGFR, ANGPT2, ANGPT1, BRAF, IGF1, MAPK12, VEGFA, GRIN1, GNAO1, EFNA3, FGF14, GNAS, KRAS, FGFR4, FGF12, FGFR3, SIPA1, FGFR2, BCAR1
	Focal adhesion	hsa04510	59/202	4.6E−07	33.9	ITGB4, FLT4, ITGA2B, PIK3CD, IGF1R, CCND1, AKT2, CAPN2, ITGB7, PDGFRB, ACTN2, PRKCB, ACTN1, PRKCA, VAV2, MYL7, COL4A2, COL4A1, MYL2, COL6A3, ITGA7, ITGA6, DOCK1, MET, SHC4, SHC2, TNXB, SHC3, LAMA2, SRC, LAMA3, PDGFB, EGFR, THBS4, PDGFD, PDGFC, MYL10, PAK6, FLNB, FYN, PIP5K1C, FLNC, LAMB3, CAV1, BRAF, PARVA, IGF1, PARVB, VEGFA, COL1A1, MAPK10, MYLPF, COL1A2, COL9A1, BCL2, COL9A3, GRB2, COL9A2, BCAR1
	PI3K-Akt signaling	hsa04151	82/341	8.5E−06	29.4	CHRM2, CDKN1A, CSF3R, HSP90AB1, ITGB4, FLT4, ITGA2B, PIK3CD, BRCA1, FGF1, FGF2, IGF1R, RPTOR, TCL1A, CCND1, CREB3L1, AKT2, CREB3L2, ITGB7, JAK3, IL6R, JAK1, PDGFRB, G6PC, TSC2, PRKCA, OSMR, COL4A2, COL4A1, DDIT4, COL6A3, ITGA7, ITGA6, SGK1, MET, CREB5, CSF1R, PHLPP1, TNXB, ATF6B, LAMA2, LAMA3, PDGFB, EGFR, THBS4, BCL2L11, RXRA, GNG7, PDGFD, PDGFC, FGF20, NGFR, ANGPT2, LAMB3, ANGPT1, NOS3, IGF1, GNG12, NFKB1, VEGFA, COL1A1, GH2, EFNA3, COL1A2, FGF14, CDK6, PPP2R2C, PPP2R2B, GNB1, PPP2R2D, COL9A1, BCL2, COL9A3, GRB2, KRAS, COL9A2, PKN1, FGFR4, PIK3AP1, FGF12, FGFR3, FGFR2
	Circadian entrainment	hsa04713	33/95	8.5E−06	27.8	RYR1, CAMK2B, RYR2, ADCY4, ITPR1, ADCY2, CACNA1D, CACNA1C, ADCY6, ADCY8, RYR3, CACNA1H, CACNA1G, CACNA1I, GRIN2A, GNG7, NOS1, PRKACA, PRKG1, KCNJ6, KCNJ9,PRKCB, PRKCA, GNG12, GRIN2C, GRIN2D, GRIN1, GNAO1, ADCY9, PER3, GNB1, NOS1AP, GNAS
	MAPK signaling	hsa04010	65/255	1.5E−05	26.7	ZAK, RASGRF2, FGF1, FGF2, RPS6KA4, MECOM, AKT2, RPS6KA2, STMN1, PRKACA, MAP3K6, MAP3K5, PDGFRB, MAP4K2, DAXX, PRKCB, IL1R2, CACNA2D1, CACNA2D3, CACNA2D2, RRAS2, PRKCA, CACNA2D4, MAP8IP3, CDC25B, TGFBR2, IL1B, MAPKAPK2, MAPT, PDGFB, CACNA1B, CACNA1A, CACNA1D, CACNA1C, NLK, CACNA1E, EGFR, CACNA1H, CACNA1G, CACNG6, CACNA1I, NTF3, GNA12, FGF20, FLNB, FLNC, CACNG2, MAP4K4, MAP2K6, NTRK1, BDNF, BRAF, NFATC1, GNG12, MAPK12, NFKB1, MAPK10, FGF14, TAOK2, GRB2, KRAS, FGFR4, FGF12, FGFR3, FGFR2
	Regulation of actin cytoskeleton	hsa04810	56/214	3.0E−05	23.4	CYFIP2, CHRM2, CYFIP1, ITGB4, ITGA2B, ITGB2, PIK3CD, WASL, ITGAE, FGF1, ITGAL, FGF2, BDKRB2, PIP4K2A, BDKRB1, PIP4K2B, ITGB7, APC2, PDGFRB, ACTN2, ACTN1, RRAS2, VAV2, MYL7, MYL2, MYH9, ITGA7, ITGA6, ARHGEF7, DOCK1, SRC, PDGFB, EGFR, SLC9A1, PDGFD,PDGFC, GNA12, FGF20, MYL10, MYH14, PAK6,PIP5K1C, MYH10,WASF2, BRAF, GNG12, BAIAP2, SSH1, MYLPF, FGF14, KRAS, FGFR4, FGF12, FGFR3, FGFR2, BCAR1

Table 2 (continued)

Contrast	Term		Overlap	Adjusted p value	Comb. score	Overlapping genes
	RAS signaling	hsa04014	56/227	3.8E−05	23	RASGRF2, FLT4, PIK3CD, FGF1, FGF2, ETS1, IGF1R, RASSF1, SYNGAP1, AKT2, PLCE1, PRKACA, PDGFRB, KSR1, PRKCB, RRAS2, PRKCA, GAB2, KSR2, ZAP70, RASA3, RAPGEF5, MET, EXOC2, SHC4, CSF1R, SHC2, SHC3, PLA2G1B, PDGFB, RASAL1, PLD1, EGFR, GRIN2A, GNG7, PDGFD, PDGFC, FGF20, PAK6, NGFR, ANGPT2, ANGPT1, IGF1, GNG12, NFKB1, VEGFA, GRIN1, MAPK10, EFNA3, FGF14, GNB1, GRB2, KRAS, FGFR4, RGL2, FGF12, FGFR3, FGFR2
	Endocytosis	hsa04144	61/259	2.4E−04	17.5	WIPF1, CLTB, WASL, AP2A2, IGF1R, CAP2B, PSD2, KIF5C, KIF5B, PSD4, PSD3, SH3GL1, ARAP2, VPS37B, ARAP1, HLA-F, HLA-G, DNM1, TGFBR2, EPN2, ACAP3, RABEP1, HGS, PARD3, RAB35, MET, RAB7A, CSF1R, SRC, VPS4A, NEDD4L, AGAP1, ASAP1, ASAP2, AGAP3, PLD1, PRKCZ, EGFR, GRK1, CYTH3, RAB11FIP1, GRK5, CLTCL1, GRK6, PIP5K1C, RAB11FIP2, RAB11FIP3, RAB11FIP4, SNX5, NTRK1, SMAD3, IQSEC. 1, SMURF1, CAV1, IQSEC. 3, WWP1, PML, EHD4, FGFR4, FGFR3, FGFR2
Irradiation (strains 1 and 2)	MAPK signaling	hsa04010	12/255	0.021	17.9	MAP2K3, CACNG6, IL1A, CACNA2D1, CACNA1B, CACNA1A, CACNA1D, FOS, FLNC, MAP3K6, MAP8IP3, MAP3K5

clones was higher than that of stable clones, indicating that RIGI is a frequent event. However, neither cytogenetic (LOY, CNVs) nor methylation (global and gene-specific) analyses revealed a significant difference between stable and unstable clones (classified by G-banding). Although this may be partially due to the fact that single-cell cloning is time-consuming and, therefore, only a limited number of clones could be analyzed, large epigenetic effects underlying RIGI can be excluded. Stochastic factors may play a major role in the cellular decision whether or not to become unstable.

Using different endpoints (number of CNVs, LOY, and radiation-associated DMPs), radiation-sensitivity differed between the two analyzed strains. This interindividual variation in radiation risk is generally assumed to be due to (epi)genetic variation modulating cellular responses to radiation-induced DNA damage [53]. Several rare cancer predisposition syndromes due to pathogenic mutations in DNA repair genes, such as ataxia-telangiectasia and Nijmegen breakage syndrome, are characterized by an increased radiosensitivity leading to adverse reactions to radiotherapy [56]. More common variants in DNA repair genes can modulate DNA damage response and radiation sensitivity [57,58]. A number of CNVs (mainly duplications), likely affecting the function of DNA repair pathways were found to be enriched in cell lines from radiation-sensitive patients with undiagnosed disease [59]. One of the genes in these radiosensitivity-associated CNVs is *CDKN1C*, an inhibitor of several G1 cyclin/Cdk complexes and cell proliferation. Mutations and paternal duplications involving *CDKN1C* cause Beckwith-Wiedemann, an overgrowth and cancer predisposition syndrome [60]. Our primary fibroblast strain 1 displayed a gain in chromosome 11p15.4 (2,904,010-2,906,824 bp) including *CDKN1C*, whereas strain 2-specific CNVs did not overlap in gene content with radiosensitivity-associated CNVs (data not shown). This *CDKN1C* copy number variation may contribute to the different radiation responses of both strains.

Because bisulfite treatment (without an additional oxidation step) cannot discriminate between 5-mC and 5-hmC, the described epigenetic changes may also include hydroxymethylation. However, using an ELISA-based assay we have previously shown that the global 5-hmC level in primary fibroblast (0.03–0.18‰) is two orders of magnitude lower than that of 5-mC (1.0–1.7%) [8]. Moreover, the 5-hmC content rapidly decreases when tissue cells are expanded in cell culture [61]. Thus, the vast majority of age- and radiation-induced changes in our study reflect gains and losses of 5-mCs.

4.2. Genetic changes

The most frequently observed cytogenetic abnormalities in unstable clones were chromatid and chromosome breaks, resulting from unrepaired double-strand breaks. The increased frequency of chromatid/chromosome breaks in tumor cells and in cells from cancer-prone individuals has been associated with compromised DNA repair [62,63]. Consistent with earlier observations [64–66], chromosomes 1, 5, 7, and 12 were frequently affected. This increased sensitivity may be related to chromosome size and interphase nuclear organization [67].

Both G-banding and FISH analyses revealed an increased rate of LOY in irradiated clones, in particular of strain 2. Clones with LOY displayed a variable proportion of cells (11–100%) without Y chromosome, suggesting that aneuploidy occurred either directly in the irradiated cell (two clones) or more frequently (9 clones) at different time points during clonal expansion. In this light, mosaic LOY can be considered as a new end point of RIGI. We did not observe a comparable mosaic loss of specific autosomes or the X chromosome in independent clones. Apart from sex determination and spermatogenesis, the Y chromosome was long considered as genetic wasteland. However, its role in complex disease pathogenesis may have been underestimated. LOY in blood cells was increasing with male age [68]. More recent studies have associated LOY in ageing men with smoking [69], Alzheimer disease [70], increased disease risk and all-cause mortality [71], shorter survival and increased cancer risk [72]. In addition, the Y is one
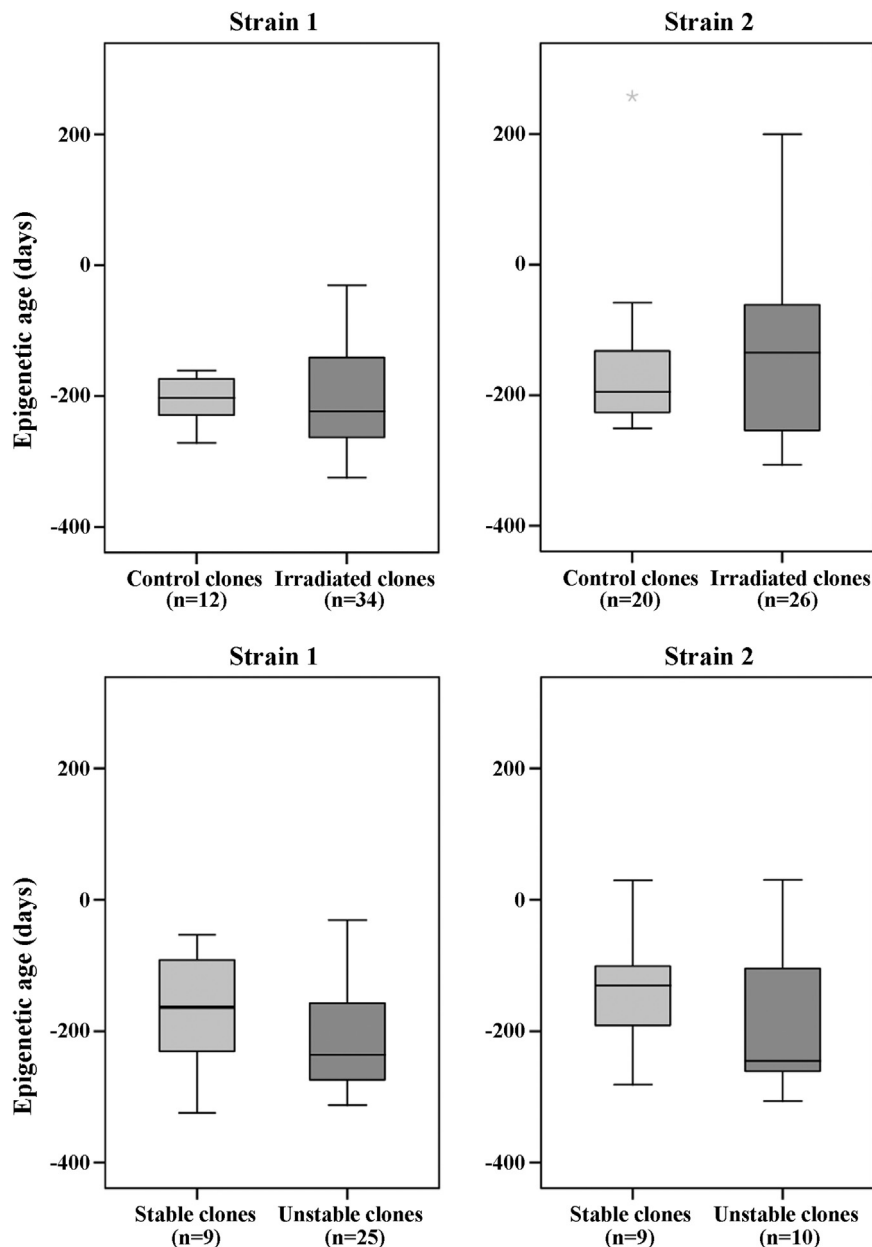
Fig. 4. Box plots showing the distribution of DNAm ages in control vs. irradiated clones and in stable vs. unstable clones in strain 1 and 2, respectively. The median is represented by a horizontal line. The bottom of the box indicates the 25th percentile, the top the 75th percentile. Outliers are shown as circles and extreme outliers as stars.

of the most commonly deleted chromosomes in a variety of cancers [73–75]. Transfer of a Y chromosome into a human prostate cancer cell line lacking this chromosome suppressed tumorigenicity in athymic nude mice [76]. *TMSB4Y* was identified as a candidate tumor suppressor on the Y chromosome [77]. Previously, it has been shown [78] that exposure to high levels of natural background radiation leads to increased frequency of microdeletions/duplications involving Y-linked genes in the AZF locus (but not their autosomal homologues) in blood cells. Collectively, these results promote the idea that radiation leaves a specific signature on the Y chromosome that may contribute to radiation-induced carcinogenesis in males.

In addition to cytogenetically visible changes, irradiation induced de novo CNVs in the progeny of exposed cells (0.46–0.7 CNVs per clone). A low number of CNVs (0.1–0.2 per control clone) is due to in vitro ageing for 20 PDs. Several previous studies described radiation-induced CNVs in immortalized or tumor cells [23,79–82]. CNV

frequency was increasing with radiation dose. The offspring of irradiated mice showed an elevated number of CNVs which arose in the paternal germ line [83]. Consistent with a study on TERT-transformed human fibroblasts [23], we observed a clustering of radiation-induced CNVs in specific chromosome regions of primary fibroblasts. The breakpoints overlapped with common fragile sites, which are induced by replication stress (aphidicolin and hydroxyurea treatment). Overall, 10 radiation-induced CNVs were congruent (overlapping or separated by < 1 Mb) between both studies. Several radiation-induced CNVs overlapped with genes (e.g. *ABCC5*, *ALDH3A1*, *BCL6*, *BTG2*, *CASP3*, *CCDC6*, *CHI3L1*, *EGFR*, *FHIT*, *MEG3*, *MIR34A*, and *PCDH7*) involved in tumorigenesis, however there was no enrichment for cancer-related pathways.

It was previously shown that FRA3B expression can be induced by high-dose X-irradiation in cancer cells [84]. We found three unstable clones and one unclassified clone with CNVs overlapping or closely

juxtaposed to the *FHIT* gene. Genetic alterations of *FHIT* caused by breaks in FRA3B are common in a variety of human cancers [84,85]. The presence of *FHIT* alterations in precancerous lesions [86–88] is consistent with a role in early stages of cancer development. The higher frequency of *FHIT* loss in lung tumors from heavy smokers compared to non-smokers promotes the idea that this gene is sensitive to environmental carcinogens [89]. *Fhit* knockout mice are prone to develop spontaneous and carcinogen-induced tumors [90,91]. Loss of *FHIT* expression leads to reduced dTTP levels and downregulation of thymidine kinase (TK1) enzyme. The resulting nucleotide imbalance causes replication stress, replication fork stalling and double-strand breaks, initiating genome instability [92–95]. We propose that disturbed caretaker function of *FHIT* through radiation-induced CNVs contributes to RIGI and radiation-induced carcinogenesis. Although FRA3B is a hotspot for radiation-induced fragility [81], the majority of irradiated clones did not exhibit detectable alterations of this region. It is plausible to assume that perturbations of different pathways are involved in destabilization of the genome after irradiation.

4.3. Epigenetic changes during in vitro ageing

Human ageing is a complex process that is influenced by genetic, environmental and behavioral factors. Nevertheless, ageing in cell culture is thought to reflect age-related changes that occur in human cells in vivo. Cellular ageing in vitro has been frequently used to study cancer and age-related pathologies [42,43]. Repetitive elements, which comprise more than half of the human genome [96], represent a surrogate marker for global DNA methylation changes [97]. DNA methylation changes between control clones (20 PDs) and the primary culture are most likely the result of in vitro ageing. Consistent with previous studies [98,99], cellular ageing was associated with global hypomethylation of ALU, LINE-1, and alpha-satellite repeats. In contrast and also consistent with the literature [100], rDNA methylation increased and, by extrapolation, nucleolar transcriptional activity decreased with ageing. Ribosome biogenesis is critical for cell metabolism, growth, and proliferation. Changes in ribosome-dependent protein synthesis play a critical role in ageing processes [101].

Methylation arrays identified 667 genes with ageing-related DMPs in both strains. These genes were enriched in pathways that are known to play a role in ageing. Fibroblast activity and focal adhesion in connective tissues decreases with age [45]. Components of the RAS signaling pathway are involved in ageing and metabolic regulation [46,51]. AMPK [44,49] and PI3K-Akt signaling [48,50] have been linked to ageing and longevity. Rodents exposed to galactose have been reported to recapitulate some features of brain ageing [52]. In a conceptually related study [47] on cultured mesenchymal stromal cells 84 CpGs in 78 genes were differentially methylated between early and late passages. Four of these 78 genes (*CASQ2*, *FGFR1*, *HK1*, and *SELPLG*) also displayed age-related DMPs in our study.

Epigenetic age is at least a passive biomarker of biological age, which is predictive of mortality [102,103], cognitive and physical functioning [104], and a number of age-related pathologies [105–107]. Consistent with the in vitro ageing model, mean DNA methylation age of control clones was higher than that of the primary culture. Interestingly, after 20 PDs there was considerable variation in epigenetic age between clones from the same primary culture, indicating epigenetic drift between clonal descendants of different cells in a culture or tissue. Since the DNAm age of clones might reflect the DNAm age of a single originating cell, our results promote the idea that single cells have greatly differing DNAm ages. Thus, the DNAm age of a tissue reflects an average across thousands of individual cells whose respective DNAm ages can differ greatly.

4.4. Epigenetic changes after radiation exposure

Methylation of ALU and alpha-satellite repeats was significantly decreased in irradiated clones, compared to controls. This global hypomethylation is to some extent reminiscent of the situation in tumor cells [17,18]. In contrast, rDNA methylation was slightly increased after irradiation. rDNA hypermethylation was also found in a variety of tumors [108,109]. However, in contrast to normal tissue, promoter methylation during tumorigenesis was not necessarily inversely correlated with rRNA expression, suggesting a more complex dysregulation of rDNA transcription [110].

Although genome-wide methylation analysis of single-copy loci revealed a marked difference in radiation sensitivity between individuals, 396 differentially methylated CpGs associated with 259 genes were found in both analyzed strains. These radiation-sensitive genes were enriched in the "MAPK signaling pathway", which is already known to play a role in radiation response [111], radiation sensitivity [112], bystander effects [113], and tumorigenesis [114]. "Pathways in cancer" and different cancer-related (Calcium, Rap1, PI3K-Alt, MAPK, and RAS) signaling pathways [115,116] were among the top 10 of 62 enriched pathways in the more sensitive strain. This promotes the idea that broad epigenetic dysregulation in the descendants of irradiated cells contributes to radiation-induced carcinogenesis.

Similar to tumor samples which are endowed with an enhanced epigenetic ageing rate, compared to their donors [37,117], irradiated clones displayed a trend increase in DNA methylation age. Blood epigenetic age has been suggested as a biomarker to predict cancer incidence and mortality [103]. Interestingly, irradiation was also associated with an increased variance and epigenetic drift between clones, compared to controls. DNAm age of unstable clones was lower than that of stable clones. Collectively, our data support the idea that radiation compromises the epigenetic maintenance system and that DNAm age tracks the cumulative work done by an epigenetic maintenance system [37].

4.5. Conclusions

Single-cell clones from primary fibroblast with intact DNA repair and cell cycle checkpoints provide an in vitro model for studying cellular ageing and delayed effects of irradiation, which both are associated with an increased cancer risk. Radiation-induced LOY and CNVs may play an important role in radiation-induced carcinogenesis. In addition, epigenetic dysregulation of cancer-relevant genes and pathways occurs in the clonal descendants of irradiated cells without direct DNA damage. The delayed (genetic and epigenetic) response to irradiation can markedly differ between individuals (fibroblast strains). In this light, it may be possible to use LOY or methylation signatures in exposed healthy cell types/tissues to predict long-term cancer risk of survivors of radiation therapy. Interestingly, it appears that DNAm age of a single cell (represented by a clone) can be quite different from the DNAm age of a tissue. Thus, DNAm age reflects the emergent property (the average) of a large number of individual cells whose respective DNAm ages can differ greatly.

Acknowledgements

Competing interests

The authors declare that no competing interests exist.

Appendix A. Supplementary material

Supplementary data associated with this article can be found in the online version at http://dx.doi.org/10.1016/j.yexcr.2018.06.034.

References

[1] S. Braunstein, J.L. Nakamura, Radiotherapy-induced malignancies: review of clinical features, pathobiology, and evolving approaches for mitigating risk, Front. Oncol. 3 (2013) 73.

[2] L. Huang, A.R. Snyder, W.F. Morgan, Radiation-induced genomic instability and its implications for radiation carcinogenesis, Oncogene 22 (2003) 5848–5854.

[3] J.B. Little, Genomic instability and bystander effects: a historical perspective, Oncogene 22 (2003) 6978–6987.

[4] L.E. Smith, S. Nagar, G.J. Kim, W.F. Morgan, Radiation-induced genomic instability: radiation quality and dose response, Health Phys. 85 (2003) 23–29.

[5] S.A. Lorimore, P.J. Coates, G.E. Scobie, G. Milne, E.G. Wright, Inflammatory-type responses after exposure to ionizing radiation in vivo: a mechanism for radiation-induced bystander effects, Oncogene 20 (2012) 7085–7095.

[6] D. Dayal, S.M. Martin, C.L. Limoli, D.R. Spitz, Hydrogen peroxide mediates the radiation-induced mutator phenotype in mammalian cells, Biochem. J. 413 (2008) 185–191.

[7] E.C. Laiakis, J.E. Baulch, W.F. Morgan, Interleukin 8 exhibits a pro-mitogenic and pro-survival role in radiation induced genomically unstable cells, Mutat. Res. 640 (2008) 74–81.

[8] A. Maierhofer, J. Flunkert, M. Dittrich, T. Müller, N. Nanda, et al., Analysis of global DNA methylation changes in primary human fibroblasts in the early phase following X-ray irradiation, PLoS One 12 (2017) e0177442.

[9] S. Kaup, V. Grandjean, R. Mukherjee, A. Kapoor, E. Keyes, et al., Radiation-induced genomic instability is associated with DNA methylation changes in cultured human keratinocytes, Mutat. Res. 597 (2006) 87–97.

[10] U. Aypar, W.F. Morgan, J.E. Baulch, Radiation-induced epigenetic alterations after low and high LET irradiations, Mutat. Res. 707 (2011) 24–33.

[11] W. Goetz, M.N. Morgan, J.E. Baulch, The effect of radiation quality on genomic DNA methylation profiles in irradiated human cell lines, Radiat. Res. 175 (2011) 575–587.

[12] M.A. Chaudhry, R.A. Omaruddin, Differential DNA methylation alterations in radiation-sensitive and -resistant cells, DNA Cell Biol. 31 (2012) 908–916.

[13] I. Koturbash, I.R. Miousse, V. Sridharan, E. Nzabarushimana, C.M. Skinner, et al., Radiation-induced changes in DNA methylation of repetitive elements in the mouse heart, Mutat. Res. 787 (2016) 43–53.

[14] I.R. Miousse, K.R. Kutanzi, I. Koturbash, Effects of ionizing radiation on DNA methylation: from experimental biology to clinical applications, Int. J. Radiat. Biol. 93 (2017) 457–469.

[15] P.A. Jones, Functions of DNA methylation: islands, start sites, gene bodies and beyond, Nat. Rev. Genet. 13 (2012) 484–492.

[16] J.A. Yoder, C.P. Walsh, T.H. Bestor, Cytosine methylation and the ecology of intragenomic parasites, Trends Genet. 13 (1997) 335–340.

[17] M. Ehrlich, Cancer-linked DNA hypomethylation and its relationship to hypermethylation, Curr. Top. Microbiol. Immunol. 10 (2006) 251–274.

[18] M. Kulis, M. Esteller, DNA methylation and cancer, Adv. Genet. 70 (2010) 27–56.

[19] D. Globisch, M. Münzel, M. Müller, S. Michalakis, M. Wagner, et al., Tissue distribution of 5-hydroxymethylcytosine and search for active demethylation intermediates, PLoS One 5 (2010) e15367.

[20] M.R. Branco, G. Ficz, W. Reik, Uncovering the role of 5-hydroxymethylcytosine in the epigenome, Nat. Rev. Genet. 13 (2012) 7–13.

[21] P.J. Hastings, J.R. Lupski, S.M. Rosenberg, G. Ira, Mechanisms of change in gene copy number, Nat. Rev. Genet. 10 (2009) 551–564.

[22] A. Shlien, D. Malkin, Copy number variations and cancer, Genome Med. 1 (2009) 62.

[23] M.F. Arlt, S. Rajendran, S.R. Birkeland, T.E. Wilson, T.W. Glover, Copy number variants are produced in response to low-dose ionizing radiation in cultured cells, Environ. Mol. Mutagen 55 (2014) 103–113.

[24] M. Seabright, A rapid banding technique for human chromosomes, Lancet 2 (1971) 971–972.

[25] J. Wirth, H.G. Nothwang, S. van der Maarel, C. Menzel, G. Borck, et al., Systematic characterisation of disease associated balanced chromosome rearrangements by FISH: cytogenetically and genetically anchored YACs identify microdeletions and candidate regions for mental retardation genes, J. Med. Genet. 36 (1999) 271–278.

[26] J.P. Schouten, C.J. McElgunn, R. Waaijer, D. Zwijnenburg, F. Diepvens, et al., Relative quantification of 40 nucleic acid sequences by multiplex ligation-dependent probe amplification, Nucleic Acids Res. 30 (2002) e57.

[27] S. Teschler, J. Gotthardt, G. Dammann, R.H. Dammann, Aberrant DNA methylation of rDNA and PRIMA1 in borderline personality disorder, Int. J. Mol. Sci. 17 (2016) 67.

[28] A. Raval, K.J. Sridhar, S. Patel, B.B. Turnbull, P.L. Greenberg, et al., Reduced rRNA expression and increased rDNA promoter methylation in CD34+ cells of patients with myelodysplastic syndromes, Blood 120 (2012) 4812–4818.

[29] T.J. Morris, L.M. Butcher, A. Feber, A.E. Teschendorff, A.R. Chakravarthy, et al., ChAMP: 450k chip analysis methylation pipeline, Bioinformatics 30 (2014) 428–430.

[30] M.J. Aryee, A.E. Jaffe, H. Corrada-Bravo, C. Ladd-Acosta, A.P. Feinberg, et al., Minfi: a flexible and comprehensive Bioconductor package for the analysis of Infinium DNA methylation microarrays, Bioinformatics 30 (2014) 1363–1369.

[31] W. Zhou, P.W. Laird, H. Shen, Comprehensive characterization, annotation and innovative use of Infinium DNA methylation beadchip probes, Nucleic Acids Res. 45 (2017) e22.

[32] A.E. Teschendorff, F. Marabita, M. Lechner, T. Bartlett, J. Tegner, et al., A beta-mixture quantile normalization method for correcting probe design bias in Illumina Infinium 450 k DNA methylation data, Bioinformatics 29 (2013) 189–196.

[33] W.E. Johnson, C. Li, A. Rabinovic, Adjusting batch effects in microarray expression data using empirical Bayes methods, Biostatistics 8 (2007) 118–127.

[34] G.K. Smyth, Linear models and empirical Bayes methods for assessing differential expression in microarray experiments, Stat. Appl. Genet. Mol. Biol. (3) (2004) (Article3).

[35] J.M. Wettenhall, G.K. Smyth, limmaGUI: a graphical user interface for linear modeling of microarray data, Bioinformatics 20 (2004) 3705–3706.

[36] Y. Benjamini, Y. Hochberg, Controlling the false discovery rate - a practical and powerful approach to multiple testing, JR Stat. Soc. B 57 (1995) 289–300.

[37] S. Horvath, DNA methylation age of human tissues and cell types, Genome Biol. 14 (2013) R115.

[38] S. Horvath, J. Oshima, G.M. Martin, A.T. Lu, A. Quach, et al., Epigenetic clock for skin and blood cells applied to Hutchinson Gilford progeria syndrome and ex vivo studies, Aging (2018) (In press).

[39] K. Debacker, R.F. Kooy, Fragile sites and human disease, Hum. Mol. Genet. 2 (2007) R150–R158.

[40] E.Y. Chen, C.M. Tan, Y. Kou, Q. Duan, Z. Wang, et al., Enrichr: interactive and collaborative HTML5 gene list enrichment analysis tool, BMC Bioinformatics 14 (2013) 128.

[41] M.V. Kuleshov, M.R. Jones, A.D. Rouillard, N.F. Fernandez, Q. Duan, et al., Enrichr: a comprehensive gene set enrichment analysis web server 2016 update, Nucleic Acids Res. 44 (2016) W90–W97.

[42] J.P. De Magalhaes, From cells to ageing: a review of models and mechanisms of cellular senescence and their impact on human ageing, Exp. Cell Res. 300 (2004) 1–10.

[43] S.M. Phipps, J.B. Berleth, L.G. Andrews, T.O. Tollefsbol, Aging cell culture: methods and observations, Methods Mol. Biol. 371 (2007) 9–19.

[44] J. Apfeld, G. O'Connor, T. McDonagh, P.S. DiStefano, R. Curtis, The AMP-activated protein kinase AAK-2 links energy levels and insulin-like signals to lifespan in C. elegans, Genes Dev. 18 (2004) 3004–3009.

[45] S.M. Arnesen, M.A. Lawson, Age-related changes in focal adhesions lead to altered cell behavior in tendon fibroblasts, Mech. Ageing Dev. 127 (2006) 726–732.

[46] V.D. Longo, Ras: the other pro-aging pathway, Sci. Aging Knowl. Environ. 39 (2004) pe36.

[47] S. Bork, S. Pfister, H. Witt, P. Horn, B. Korn, et al., DNA methylation pattern changes upon long-term culture and aging of human mesenchymal stromal cells, Aging Cell 9 (2010) 54–63.

[48] D. Heras-Sandoval, E. Avila-Muñoz, C. Arias, The phosphatidylinositol 3-kinase/mTor pathway as a therapeutic target for brain aging and neurodegeneration, Pharmaceuticals 4 (2011) 1070–1087.

[49] A. Salminen, K. Kaarniranta, AMP-activated protein kinase (AMPK) controls the aging process via an integrated signaling network, Ageing Res. Rev. 11 (2012) 230–241.

[50] C. O'Neill, PI3-kinase/Akt/mTOR signaling: impaired on/off switches in aging, cognitive decline and Alzheimer's disease, Exp. Gerontol. 48 (2013) 647–653.

[51] C. Slack, Ras signaling in aging and metabolic regulation, Nutr. Healthy Aging 4 (2017) 195–205.

[52] T. Shwe, W. Pratchayasakul, N. Chattipakorn, S.C. Chattipakorn, Role of D-galactose-induced brain aging and its potential used for therapeutic interventions, Exp. Gerontol. 101 (2018) 13–36.

[53] K. Schnarr, I. Dayes, J. Sathya, D. Boreham, Individual radiosensitivity and its relevance to health physics, Dose Response 5 (2007) 333–348.

[54] J.G. Herman, S.B. Baylin, Gene silencing in cancer in association with promoter hypermethylation, N. Engl. J. Med. 349 (2003) 2042–2054.

[55] A. Karakosta, C. Golias, A. Charalabopoulos, D. Peschos, A. Batistatou, et al., Genetic models of human cancer as a multistep process. paradigm models of colorectal cancer, breast cancer, and chronic myelogenous and acute lymphoblastic leukaemia, J. Exp. Clin. Cancer Res. 24 (2005) 505–514.

[56] J.M. Pollard, R.A. Gatti, Clinical radiation sensitivity with DNA repair disorders: an overview, Int. J. Radiat. Oncol. Biol. Phys. 74 (2009) 1323–1331.

[57] G. Iarmarcovai, S. Bonassi, A. Botta, R.A. Baan, T. Orsière, Genetic polymorphisms and micronucleus formation: a review of the literature, Mutat. Res. 658 (2008) 215–233.

[58] N.K. Bolegenova, B.O. Bekmanov, L.B. Djansugurova, R.I. Bersimbaev, S.A. Salama, et al., Genetic polymorphisms and expression of minisatellite mutations in a 3-generation population around the Semipalatinsk nuclear explosion test-site, Kazakhstan, Int J. Hyg. Environ. Health 212 (2009) 654–660.

[59] X. Li, J. Zhou, S.A. Nahas, H. Wan, H. Hu, et al., Common copy number variations in fifty radiosensitive cell lines, Genomics 99 (2012) 96–100.

[60] B. Baskin, S. Choufani, Y.A. Chen, C. Shuman, N. Parkinson, et al., High frequency of copy number variations (CNVs) in the chromosome 11p15 region in patients with Beckwith-Wiedemann syndrome, Hum. Genet. 133 (2014) 321–330.

[61] C.E. Nestor, R. Ottaviano, J. Reddington, D. Sproul, D. Reinhardt, et al., Tissue type is a major modifier of the 5-hydroxymethylcytosine content of human genes, Genome Res. 22 (2012) 467–477.

[62] R. Parshad, K.K. Sanford, G.M. Jones, Chromatid damage after G2 phase X-irradiation of cells from cancer-prone individuals implicates deficiency in DNA repair, Proc. Natl. Acad. Sci. USA 80 (1983) 5612–5616.

[63] R. Parshad, R. Gantt, K.K. Sanford, G.M. Jones, Chromosomal radiosensitivity of human tumor cells during the G2 cell cycle period, Cancer Res. 44 (1984) 5577–5582.

[64] M. Bauchinger, G. Götz, Distribution of radiation induced lesions in human chromosomes and dose-effect relation analysed with G-banding, Radiat. Environ. Biophys. 16 (1979) 355–366.

[65] Y. Kano, J.B. Little, Site-specific chromosomal rearrangements induced in human diploid cells by X-irradiation, Cytogenet Cell Genet. 41 (1986) 22–29.

[66] L. Barrios, R. Miro, M.R. Caballin, C. Fuster, F. Guedea, A. Subias, J. Egozcue, Cytogenetic effects of radiotherapy. Breakpoint distribution in induced chromosome aberrations, Cancer Genet. Cytogenet 41 (1989) 61–70.

[67] S. Cigarran, L. Barrios, J.F. Barquinero, M.R. Caballin, M. Ribas, et al., Relationship between the DNA content of human chromosomes and their involvement in radiation-induced structural aberrations, analysed by painting, Int. J. Radiat. Biol. 74 (1998) 449–455.

[68] M. Guttenbach, B. Koschorz, U. Bernthaler, T. Grimm, M. Schmid, Sex chromosome loss and aging: in situ hybridization studies on human interphase nuclei, Am. J. Hum. Genet. 57 (1995) 1143–1150.

[69] J.P. Dumanski, C. Rasi, M. Lonn, H. Davies, M. Ingelsson, et al., Mutagenesis. Smoking is associated with mosaic loss of chromosome Y, Science 347 (2015) 81–83.

[70] J.P. Dumanski, J.C. Lambert, C. Rasi, V. Giedraitis, H. Davies, et al., Mosaic loss of chromosome Y in blood is associated with Alzheimer disease, Am. J. Hum. Genet. 98 (2016) 1208–1219.

[71] L.A. Forsberg, Loss of chromosome Y (LOY) in blood cells is associated with increased risk for disease and mortality in aging men, Hum. Genet. 136 (2017) 657–663.

[72] L.A. Forsberg, C. Rasi, N. Malmqvist, H. Davies, S. Pasupulati, et al., Mosaic loss of chromosome Y in peripheral blood is associated with shorter survival and higher risk of cancer, Nat. Genet. 46 (2014) 624–628.

[73] E. Lippert, G. Etienne, M.J. Mozziconacci, S. Laibe, C. Gervais, et al., Loss of the Y chromosome in Philadelphia-positive cells predicts a poor response of chronic myeloid leukemia patients to imatinib mesylate therapy, Haematologica 95 (2010) 1604–1607.

[74] S. Minner, A. Kilgue, P. Stahl, S. Weikert, M. Rink, et al., Y chromosome loss is a frequent early event in urothelial bladder cancer, Pathology 42 (2010) 356–359.

[75] E. Chapiro, I. Antony-Debre, N. Marchay, C. Parizot, C. Lesty, et al., Sex chromosome loss may represent a disease-associated clonal population in chronic lymphocytic leukemia, Genes Chromosomes Cancer 53 (2014) 240–247.

[76] S. Vijayakumar, D. Garcia, C.H. Hensel, M. Banerjee, T. Bracht, et al., The human Y chromosome suppresses the tumorigenicity of PC-3, a human prostate cancer cell line, in athymic nude mice, Genes Chromosomes Cancer 44 (2005) 365–372.

[77] H.Y. Wong, G.M. Wang, S. Croessman, D.J. Zabransky, D. Chu, et al., TMSB4Y is a candidate tumor suppressor on the Y chromosome and is deleted in male breast cancer, Oncotarget 6 (2015) 44927–44940.

[78] S. Premi, J. Srivastava, S.P. Chandy, S. Ali, Unique signatures of natural background radiation on human Y chromosomes from Kerala, India, PLoS One 4 (2009) e4541.

[79] H.M. Kang, J.J. Jang, C. Langford, S.H. Shin, S.Y. Park, et al., DNA copy number alterations and expression of relevant genes in mouse thymic lymphomas induced by gamma-irradiation and N-methyl-N-nitrosourea, Cancer Genet. Cytogenet. 166 (2006) 27–35.

[80] R.R. Kimmel, S. Agnani, Y. Yang, R. Jordan, J.L. Schwartz, DNA copy-number instability in low-dose gamma-irradiated TK6 lymphoblastoid clones, Radiat. Res. 169 (2008) 259–269.

[81] A. Muradyan, K. Gilbertz, S. Stabentheiner, S. Klause, H. Madle, et al., Acute high-dose X-radiation-induced genomic changes in A549 cells, Radiat. Res. 175 (2011) 700–707.

[82] H. Zitzelsberger, K. Unger, DNA copy number alterations in radiation-induced thyroid cancer, Clin. Oncol. (R. Coll. Radiol.) 23 (2011) 289–296.

[83] A.B. Adewoye, S.J. Lindsay, Y.E. Dubrova, M.E. Hurles, The genome-wide effects of ionizing radiation on mutation induction in the mammalian germline, Nat. Commun. 6 (2015) 6684.

[84] S.G. Durkin, R.L. Ragland, M.F. Arlt, J.G. Mulle, S.T. Warren, et al., Replication stress induces tumor-like microdeletions in FHIT/FRA3B, Proc. Natl. Acad. Sci. USA 105 (2008) 246–251.

[85] C.E. Waters, J.C. Saldivar, S.A. Hosseini, K. Huebner, The FHIT gene product: tumor suppressor and genome "caretaker", Cell Mol. Life Sci. 71 (2014) 4577–4587.

[86] K.M. Fong, E.J. Biesterveld, A. Virmani, I. Wistuba, Y. Sekido, et al., FHIT and FRA3B 3p14.2 allele loss are common in lung cancer and preneoplastic bronchial lesions and are associated with cancer-related FHIT cDNA splicing aberrations, Cancer Res. 57 (1997) 2256–2267.

[87] G. Sozzi, U. Pastorino, L. Moiraghi, E. Tagliabue, F. Pezzella, et al., Loss of FHIT function in lung cancer and preinvasive bronchial lesions, Cancer Res. 58 (1998) 5032–5037.

[88] G. Guler, A. Uner, N. Guler, S.Y. Han, D. Iliopoulos, et al., Concordant loss of fragile gene expression early in breast cancer development, Pathol. Int. 55 (2005) 471–478.

[89] G. Sozzi, L. Sard, L. De Gregorio, A. Marchetti, K. Musso, et al., Association between cigarette smoking and FHIT gene alterations in lung cancer, Cancer Res. 57 (1997) 2121–2123.

[90] L.Y. Fong, V. Fidanza, N. Zanesi, L.F. Lock, L.D. Siracusa, et al., Muir-Torre-like syndrome in Fhit-deficient mice, Proc. Natl. Acad. Sci. USA 97 (2000) 4742–4747.

[91] N. Zanesi, V. Fidanza, L.Y. Fong, R. Mancini, T. Druck, et al., The tumor spectrum in FHIT-deficient mice, Proc. Natl. Acad. Sci. USA 98 (2001) 10250–10255.

[92] J.C. Saldivar, S. Miuma, J. Bene, S.A. Hosseini, H. Shibata, et al., Initiation of genome instability and preneoplastic processes through loss of Fhit expression, PLoS Genet. 8 (2012) e1003077.

[93] S. Miuma, J.C. Saldivar, J.R. Karras, C.E. Waters, C.A. Paisie, et al., Fhit deficiency-induced global genome instability promotes mutation and clonal expansion, PLoS One 8 (2013) e80730.

[94] I. Hazan, T.G. Hofmann, R.I. Aqeilan, Tumor suppressor genes within common fragile sites are active players in the DNA damage response, PLoS Genet 12 (2016) e1006436.

[95] C.A. Paisie, M.S. Schrock, J.R. Karras, J. Zhang, S. Miuma, et al., Exome-wide single-base substitutions in tissues and derived cell lines of the constitutive Fhit knockout mouse, Cancer Sci. 107 (2016) 528–535.

[96] A.P. De Koning, W. Gu, T.A. Castoe, M.A. Batzer, D.D. Pollock, Repetitive elements may comprise over two-thirds of the human genome, PLoS Genet. 7 (2011) e1002384.

[97] A.S. Yang, M.R. Estecio, K. Doshi, Y. Kondo, E.H. Tajara, et al., A simple method for estimating global DNA methylation using bisulfite PCR of repetitive DNA elements, Nucleic Acids Res. 32 (2004) e38.

[98] A.A. Johnson, K. Akman, S.R. Calimport, D. Wuttke, A. Stolzing, et al., The role of DNA methylation in aging, rejuvenation, and age-related disease, Rejuvenation Res. 15 (2012) 483–494.

[99] M. Zampieri, F. Ciccarone, R. Calabrese, C. Franceschi, A. Bürkle, et al., Reconfiguration of DNA methylation in aging, Mech. Ageing Dev. 151 (2015) 60–70.

[100] A. Machwe, D.K. Orren, V.A. Bohr, Accelerated methylation of ribosomal RNA genes during the cellular senescence of Werner syndrome fibroblasts, FASEB J. 14 (2000) 1715–1724.

[101] S.I. Rattan, Synthesis, modifications, and turnover of proteins during aging, Exp. Gerontol. 31 (1996) 33–47.

[102] R.E. Marioni, S. Shah, A.F. McRae, B.H. Chen, E. Colicino, et al., DNA methylation age of blood predicts all-cause mortality in later life, Genome Biol. 16 (2015) 25.

[103] Y. Zheng, B.T. Joyce, E. Colicino, L. Liu, W. Zhang, et al., Blood epigenetic age may predict cancer incidence and mortality, EBioMedicine 5 (2016) 68–73.

[104] R.E. Marioni, S. Shah, A.F. McRae, S.J. Ritchie, G. Muniz-Terrera, et al., The epigenetic clock is correlated with physical and cognitive fitness in the Lothian Birth Cohort 1936, Int. J. Epidemiol. 44 (2015) 1388–1396.

[105] M.E. Levine, A.T. Lu, D.A. Bennett, S. Horvath, Epigenetic age of the pre-frontal cortex is associated with neuritic plaques, amyloid load, and Alzheimer's disease related cognitive functioning, Aging 7 (2015) 1198–1211.

[106] L. Perna, Y. Zhang, U. Mons, B. Holleczek, K.U. Saum, et al., Epigenetic age acceleration predicts cancer, cardiovascular, and all-cause mortality in a German case cohort, Clin. Epigenet. 8 (2016) 64.

[107] A. Maierhofer, J. Flunkert, J. Oshima, G.M. Martin, T. Haaf, et al., Accelerated epigenetic aging in Werner syndrome, Aging 9 (2017) 1143–1152.

[108] P.S. Yan, F.J. Rodriguez, D.E. Laux, M.R. Perry, S.B. Standiford, et al., Hypermethylation of ribosomal DNA in human breast carcinoma, Br. J. Cancer 82 (2000) 514–517.

[109] M.W. Chan, S.H. Wei, P. Wen, Z. Wang, D.E. Matei, et al., Hypermethylation of 18S and 28S ribosomal DNAs predicts progression-free survival in patients with ovarian cancer, Clin. Cancer Res. 11 (2005) 7376–7383.

[110] G. Karahan, N. Sayar, G. Gozum, B. Bozkurt, O. Konu, et al., Relative expression of rRNA transcripts and 45S rDNA promoter methylation status are dysregulated in tumors in comparison with matched-normal tissues in breast cancer, Oncol. Rep. 33 (2015) 3131–3145.

[111] P. Dent, A. Yacoub, P.B. Fisher, M.P. Hagan, S. Grant, MAPK pathways in radiation responses, Oncogene 22 (2003) 5885–5896.

[112] H.B. Forrester, J. Li, T. Leong, M.J. McKay, C.N. Sprung, Identification of a radiation sensitivity gene expression profile in primary fibroblasts derived from patients who developed radiotherapy-induced fibrosis, Radiother. Oncol. 111 (2014) 186–193.

[113] F.M. Lyng, P. Maguire, B. McClean, C. Seymour, C. Mothersill, The involvement of calcium and MAP kinase signaling pathways in the production of radiation-induced bystander effects, Radiat. Res. 165 (2006) 400–409.

[114] M. Burotto, V.L. Chiou, J.M. Lee, E.C. Kohn, The MAPK pathway across different malignancies: a new perspective, Cancer 120 (2014) 3446–3456.

[115] X.X. Wang, F.H. Xiao, Q.G. Li, J. Liu, Y.H. He, et al., Large-scale DNA methylation expression analysis across 12 solid cancers reveals hypermethylation in the calcium-signaling pathway, Oncotarget 8 (2017) 11868–11876.

[116] Y.L. Zhang, R.C. Wang, K. Cheng, B.Z. Ring, L. Su, Roles of Rap1 signaling in tumor cell migration and invasion, Cancer Biol. Med. 14 (2017) 90–99.

[117] G. Hannum, J. Guinney, L. Zhao, L. Zhang, G. Hughes, et al., Genome-wide methylation profiles reveal quantitative views of human aging rates, Mol. Cell 49 (2013) 359–367.